Earth Planets Space, **58**, 305–314, 2006

Stress change prior to the major events in the 1989 earthquake swarm off the eastern Izu Peninsula, Japan

Hironori Kawakata[1], Hiroshi Ogasawara[2], Shoji Sekiguchi[3], Shizuka Uyama[4], and Kazuo Mino[2]

[1]*Disaster Prevention Research Institute, Kyoto University, Uji, Kyoto 611-0011, Japan*
[2]*Faculty of Science and Engineering, Ritsumeikan University, Kusatsu, Shiga 525-8577, Japan*
[3]*Solid Earth Science Division, National Research Institute for Earth Science and Disaster Prevention, Tsukuba, Ibaraki 305-0006, Japan*
[4]*Faculty of Science and Engineering, Ritsumeikan University (Graduated), Kusatsu, Shiga 525-8577, Japan*

(Received July 7, 2005; Revised September 12, 2005; Accepted September 16, 2005; Online published March 10, 2006)

We investigate a temporal change in a stress parameter of earthquakes that occurred in the 1989 swarms off the eastern Izu Peninsula in Japan. We use the energy index (*EI*), which have been monitored in deep South African gold mines for predicting major events, as an estimate of apparent stress that is proportional to the ratio of seismic energy (E) to seismic moment (Mo). *EI* measures an excess or shortage in E with respect to the empirical relationship between E and Mo. We check that *EI* is almost proportional to the apparent stress for the ranges of Mo and frequency for our analysis, although E is underestimated due to the artifact of limited frequency band of monitoring. The largest events ($M = 5.2$ and 5.5) took place off the tip of a vertical crack, which opened associated with magma intrusion. While the opening continued to load the source areas of the M 5.2 and 5.5, we find significant decrease in *EI* prior to the events. Based on the experimental result that the stress decreases when yielding takes place prior to final failure, we interpret this observation as yielding in the vicinity of the large earthquake hypocenters, following a rapid increase in stress caused by magma intrusion.
Key words: Decrease in stress, precursor, energy index, earthquake development process, earthquake swarm.

1. Introduction

Stress state is one of the most important parameters for describing the physical processes of earthquakes. In particular, learning its temporal variation in seismic source regions of the Earth's crust just prior to seismic events is essential for understanding the earthquake development process. In a spring-block system (Burridge and Knopoff, 1967; Carlson and Langer, 1989) that can be interpreted as an earthquake model, the instability depends on the effective stiffness of system k, and begins when

$$\partial\tau/\partial\delta = k, \tag{1}$$

where τ and δ are shear stress and relative slip, respectively (Rudnicki, 1988). Instability occurs only after the (quasi-) stable stress decrease, since k is always positive. Laboratory experiments with granite samples confirm that instability (dynamic rupture) occurs after peak stress, both in triaxial fracture (e.g., Kawakata *et al*., 1999) and in frictional sliding (e.g., Ohnaka *et al*., 1986).

For natural earthquakes, however, there have been few studies of such phenomena, since there are few ways to measure the stress state in the source region. In situ stress can be estimated by utilizing a borehole (e.g., Brudy *et al*., 1997) or drill cores (e.g., Teufel, 1983; Simmons *et al*., 1974; Zang *et al*., 1996), but as yet, only KTB research well extends to seismogenic depths (Brudy *et al*., 1997; Zang *et al*., 1996). Alternatively, we can indirectly estimate the stress state of a source region by analyzing the seismograms of preceding small earthquakes. For this to be possible, we need sufficient earthquakes (a large number of foreshocks or a high level of background seismicity). We also need to remove path and site effects from the seismograms. For this kind of analysis to work, we need high dynamic range of seismograms from earthquakes spanning a wide magnitude range, recorded close to the epicenters.

Stress drop and apparent stress have frequently been used as stress parameters. To accurately determine the stress drop, however, an accurate estimation of a corner frequency is needed, which is obtained only with a discrete Fourier spectrum with the frequency range wide enough to cover the corner frequency. In other words, we must have an enough number of samples within phase duration, but this is not always easy in case of small earthquakes. The apparent stress is another measure of stress state defined by Wyss and Brune (1968), which is proportional to the ratio of the seismic energy to the seismic moment. However, Ide and Beroza (2001) pointed out that the apparent stress tends to be underestimated for small earthquakes due to an artifact, if the effective frequency range is not wide enough.

In deep gold mines in South Africa, van Aswegen and Butler (1993) proposed the energy index (*EI*) as a stress parameter that is calculated from seismic moment and seismic energy. Changes in *EI* have been observed prior to major seismic events induced by mining, and this has contributed to the prediction of major seismic events (Mendecki, 1997). Here we demonstrate the *EI* is almost proportional to the

Copyright © The Society of Geomagnetism and Earth, Planetary and Space Sciences (SGEPSS); The Seismological Society of Japan; The Volcanological Society of Japan; The Geodetic Society of Japan; The Japanese Society for Planetary Sciences; TERRAPUB.

full-band apparent stress for the ranges of magnitude and data sampling frequency for our analysis.

In the present study, we apply the method used in South Africa to the 1989 earthquake swarm off the eastern Izu Peninsula in Japan. Around the Izu Peninsula, which is covered by a dense network of seismic and geodetic stations, a number of volcanic eruptions and related seismic swarms have been recorded. We take into account whole-path anelastic attenuation, radiation pattern, and fault orientation, and we estimate the temporal variation of the stress state from EI, prior to the two largest earthquakes ($M = 5.2$ and 5.5) in the swarm. We then compare our results with strain and tilt data observed in a surrounding region.

2. The 1989 Earthquake Swarm Off the Eastern Izu Peninsula

Several seismic swarm activities have occurred around the Izu Peninsula, Central Japan, since the 1974 Izu-Hanto-Oki earthquake. The westernmost and shallowest seismic swarm around the Izu Peninsula for the 15 years (1974–1989) began at the end of June, 1989 (Okada and Yamamoto, 1991).

The hypocenters of earthquakes located by National Research Institute for Earth Science and Disaster Prevention (NIED) from July 1 to July 15 are shown in Figs. 1 and 2. On the morning of July 4, the tilt rate, its direction, and the rate of dilatation drastically changed at station ITO (Yamamoto *et al*., 1991; Earthquake Prediction Information Division, 1990). At the same time, there was a sudden increase in seismic activity to the highest level ever observed in the region (Matsumura *et al*., 1991). The seismicity level remained high for three days, and the two largest earthquakes ($M = 5.2$ and 5.5) in the swarm took place at 0:01 (LT) on July 7 and at 11:09 (LT) on July 9, respectively. Both earthquakes have right-lateral strike-slip focal mechanisms (NIED, Fig. 1), and the preferred fault planes are shown in Fig. 1. The M 5.2 earthquake had relatively few aftershocks to usual earthquakes such as the M 5.5 earthquake (Fig. 2). Fukuyama *et al*. (1991) found that the rupture of M 5.5 earthquake began near a strong asperity. Four days after the M 5.5 earthquake, on July 13, a submarine volcanic eruption occurred, about 3 km offshore of Ito City (at Teishi knoll).

We divide the swarm activity into eastern and western groups, centered on 139.1°E longitude, based on characteristics observed by Matsumura *et al*. (1991). Matsumura *et al*. (1991) studied the distribution and migration of the active seismic zone, and found that the swarm activity in the eastern group was closely related to magma intrusion. They also concluded that the relatively low activity in the western group, off the tip of the magma intrusion area, where the M 5.2 and 5.5 events occurred, was of tectonic, not volcanic, origin.

During the swarm, a vertical crack striking NW-SE (the white line in Fig. 1) was opened by intruding magma to a thickness of about 1 m (Okada and Yamamoto, 1991). The thickness of this intruded vertically-opening crack is comparable to that of tabular mining in deep South African gold mines and an $M > 4$ event takes place on an existing fault when the mined area at the proximity of the fault reaches

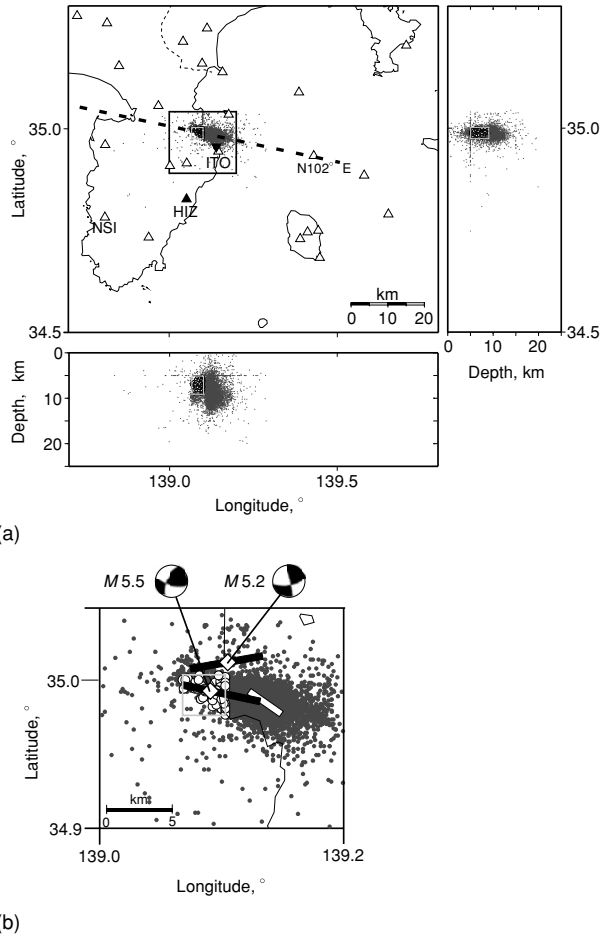

Fig. 1. Hypocenter distribution for the 1989 Earthquake Swarm off the eastern Izu Peninsula from July 1 to July 15, 1989. (a) Seismogram stations operated by NIED, including NSI (open triangles), dilatometer station HIZ of the Japan Meteorological Agency (solid triangle), and NIED tiltmeter station ITO (solid reverse triangle). A broken line shows the strike of the M 5.5 earthquake. A light gray rectangle in each panel represents the outer frame of our target region. (b) Enlarged epicenter distribution of the region outlined by an open black square in (a). Open circles represent the analyzed earthquakes. The black lines with open diamonds represent the fault strike of the M 5.2 earthquake on July 7 and the M 5.5 earthquake on July 9. The epicenters of these earthquakes that are represented by open diamonds were at 34.991°N, 139.088°E and at 35.012°N, 139.105°E, and the focal depths at 6.8 km and 3.6 km, based on NIED analysis, respectively. The focal mechanism projections for the M 5.2 earthquake and M 5.5 earthquake determined by NIED are also shown. The white line shows the vertical open crack of the submarine eruption described by Okada and Yamamoto (1991).

on the order of 1 km^2 (e.g., COMRO, 1988). The shear faultings of the major earthquakes (the black lines in Fig. 1) were closely related to the opening of the vertical crack, the geometrical situation being similar to major events in deep mines that occur along faults adjacent to excavations (e.g., Gibowicz and Kijko, 1994). In addition, the volumetric strain rate change at HIZ station (Fig. 1) during the intrusion from $\sim 10^{-7}$ /day to $\sim 10^{-6}$ /day (Earthquake Prediction Information Division, 1990) is comparable to that at the distance less than 100 m from a hypocenter of $M > 2$ in deep South African gold mines for several days prior to this earthquake during mining at the proximity of the fault (Ogasawara *et al*., 2005). We therefore use this South African analogy to determine whether there was any change prior

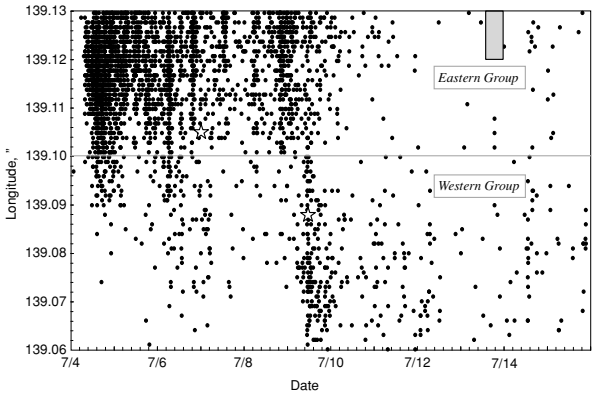

Fig. 2. The temporal variation in hypocenter (longitudinal projection) for all the events detected by NIED that occurred around the target region. Latitude range is the same as the target region. Solid circles, open stars, and an enclosed gray square indicate the projected hypocenters, the largest earthquakes (M 5.2 and 5.5), and a submarine volcanic eruption at Teishi knoll, respectively.

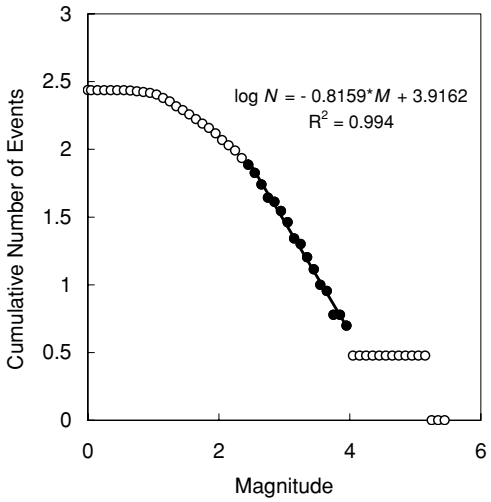

Fig. 3. The magnitude-frequency relationship for the earthquakes occurred in the target region. Solid circles represent the cumulative number of events from $M > 2.4$ to $M > 4.0$.

to the major earthquakes at Izu, similar to those detected in the deep South African gold mines.

3. Data

We use three components of the velocity seismograms recorded at NIED station NSI (Fig. 1) from July 1 to July 15, 1989. NSI is a borehole seismograph station 448 m deep in a tuff layer with a relatively high P-wave velocity of around 4500–5200 m/s (Suzuki *et al.*, 1981). We choose station NSI because of the dynamic range of its seismographs and its signal-to-noise ratio. We only analyze P-wave because S-wave tends to often be clipped. Most of the earthquakes we analyze are strike slip events and NSI is best located because the site is most insensitive to the fluctuation of the orientation of the analyzed strike-slip-faulting. Seismographs employed at NSI have a natural frequency around 4.2 Hz, and their output signals were digitally recorded at the sampling frequency of 80 Hz after band-pass filtering between 0.01 Hz and 20 Hz. Events closely related to magma intrusion must be excluded from this analysis, and the target region should include the fault zone of the M 5.2 and 5.5 earthquakes, as we are interested in the state of stress in the source region of these earthquakes. Considering the source radius of $\sim$ 3 km for M 5.5 event and lower hypocenter accuracy in depth, we select the target region for the western group 3 km across, 4 km in depth, whose easternmost end, northernmost end, and uppermost end are 139.1°E longitude, 35.005°N latitude, and 5 km, respectively (light gray rectangles in Fig. 1), then the hypocenter of the M 5.5 earthquake is located around the center of target region. As the M 5.2 epicenter was located near the northeastern corner of our target region, we pay attention to how the stress state in the target region was related to the occurrence of this earthquake. Carefully checking that the magnitude-frequency relationship satisfies the Gutenberg-Richter's law (Fig. 3), we use the lower magnitude limit of $M = 2.4$ in our analysis so that we exclude only a few events. The upper limit of $M = 3.5$ is specified so that the P-waves are not clipped. Seventy-three earthquakes (Fig. 1) are selected in this manner (no events occurred in the target region before July 4). Their hypocenters, shown in Fig. 1, were determined by NIED from both P- and S-arrivals recorded at over thirty stations. The average horizontal and vertical errors in their hypocenter locations are 0.4 km and 1.0 km, respectively, and at most 0.6 km and 1.9 km, respectively.

4. Waveform Analysis

4.1 Waveform correction

A recorded seismogram $U(t)$ can be represented as

$$U(t) = S(t) * E(t) * A(t) * L(t) * I(t), \qquad (2)$$

where $S(t)$, $E(t)$, $A(t)$, $L(t)$, and $I(t)$ are the signal from the seismic source, the elastic path effect, the anelastic path effect, the site effect, and the instrument response, respectively. In Eq. (2), $*$ denotes a convolution operation. We must remove $A(t)$, $L(t)$, and $I(t)$, since $S(t) * E(t)$ is required to estimate E and Mo. First, we remove the instrument response $I(t)$ by convolving its inverse filter with the seismogram after the seismogram was preliminary filtered by a sixth-order Bessel band-pass filter with a band frequency from 0.5 Hz to 20 Hz. We do not need to remove the site effect $L(t)$ to investigate the temporal variation of the source parameters, because we analyze seismograms recorded at a single station NSI and do not compare them with those recorded at any other stations. The station NSI is located about 35 km from the active seismic and volcanic region, and so the temporal change in site environment at NSI can be considered negligible.

The Fourier spectrum of the anelastic path effect $U(f)$ can be expressed in terms of the anelastic attenuation factor of the P-wave Q_P (Brune, 1970):

$$U(f) = \frac{Ao \exp(-\frac{\pi R f}{\alpha Q_P})}{(1 + f/f_c)^2}, \qquad (3)$$

where R, f, f_c, and α are hypocentral distance, frequency, corner frequency, and P-wave velocity, respectively. The Fourier spectrum of displacement waveform propagation in

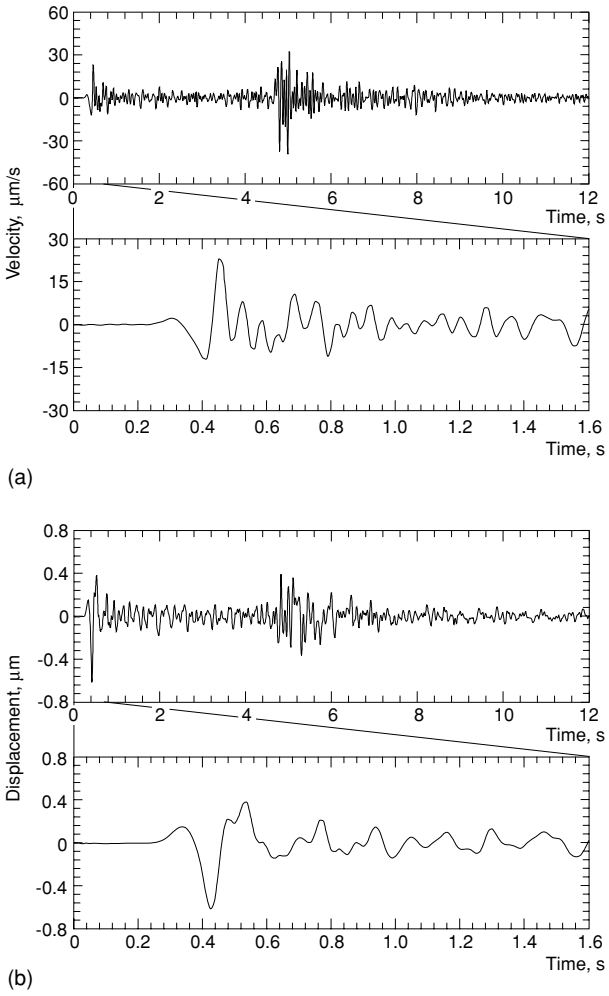

Fig. 4. Radial component of velocity and displacement waveforms for a typical earthquake (21:58 on July 9). (a) Full trace of radial-component velocity waveform (top) and its initial portion (bottom). (b) Full trace of radial-component displacement waveform (top) and its initial portion (bottom).

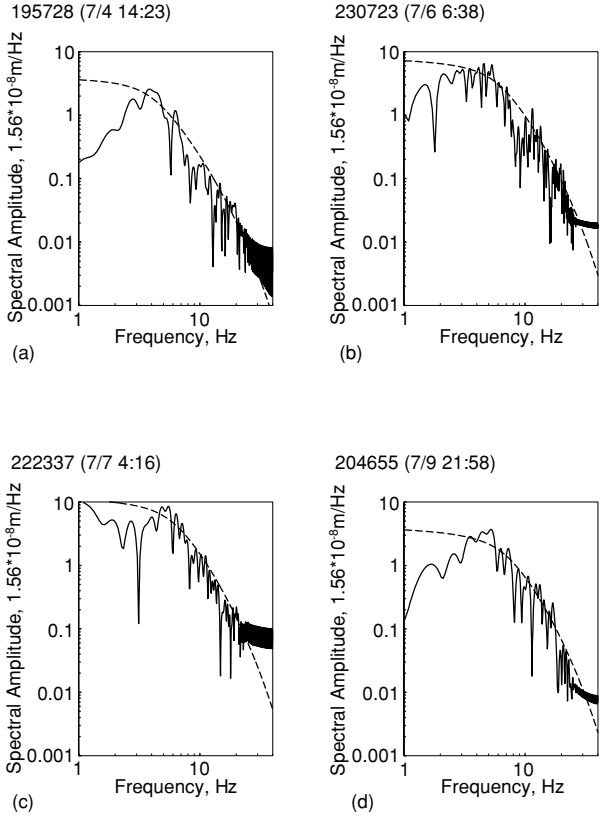

Fig. 5. Displacement spectrum of a *P*-wave 1.6-s window for some earthquakes that occurred in various periods. A broken curve in each window shows the synthetic spectrum with whole-path Q_P of 200.

an elastic medium will decay in inverse proportion to the second power of the frequency at high frequencies (e.g., Brune, 1970; Madariaga, 1976). The whole-path Q_P is estimated by fitting the spectra with Eq. (3). We integrate the velocity waveform of radial component (Fig. 4(a)) to displacement (Fig. 4(b)), and then calculate the Fourier spectrum using 1.6-s time windows from 0.2 s before the first *P*-pulse arrival (Fig. 5). We model the spectra using Eq. (3) to determine Q_P. The values of whole-path Q_P are estimated to be around 200 for all the events (dashed lines in Fig. 5). Using the second form of the linear absorption law of Azimi *et al.* (1968) with $Q_P = 200$, the impulse response is calculated, and then, all the velocity waveforms are deconvolved with it before all of the further analyses.

4.2 Seismic moment and seismic energy

The scalar seismic moment *Mo* is estimated from the relation (Keilis-Borok, 1960):

$$Mo = \frac{4\pi\rho\alpha^3 R}{F^P} Ao, \tag{4}$$

where ρ and F^P are density of the medium and the radiation pattern of the *P*-wave, using a radial component of displacement seismograms with 1.6-s time window from 0.2 s before the first *P*-pulse arrival.

The seismic energy *E* is calculated from a radial component of velocity seismograms by the relation (Boatwright, 1980; Iio, 1986):

$$E = \int_{R/\alpha}^{R/\alpha+\Delta t} 4\pi R^2 \rho\alpha \left(\frac{\dot{u}_r(\mathbf{x}, t)}{F^P}\right)^2 dt, \tag{5}$$

where $\dot{u}_r$ is the radial component of velocity waveform, using the same time window (Δt) of the direct *P*-wave velocity waveform that is used for estimating *Mo*.

F^P varies with the focal mechanism and the location of the hypocenter. We calculate F^P using the focal mechanisms (determined by NIED) and equation (4.84) in Aki and Richards (1980). The F^P is less than 0.35 for 22 earthquakes that have focal mechanisms very different to that of the *M* 5.5 earthquake ($F^P = 0.47$). *EI* becomes more sensitive to errors in F^P as F^P decreases, because *EI* is inversely proportional to F^P. Therefore, we exclude these 22 events, and used only the 51 events with $F^P > 0.35$. We assume that $\rho = 2840$ kg/m^3 and $\alpha = 5500$ m/s, and calculate the seismic moment and the seismic energy using Eqs. (4) and (5) (Table 1, Fig. 6).

5. Energy Index as a Stress Parameter

The stress drop ($\Delta\sigma$), which can be estimated from the relation (Madariaga, 1976; Eshelby, 1957):

$$\Delta\sigma \approx \frac{44 Mo \cdot f_c^3}{\alpha^3}, \tag{6}$$

Table 1. Estimated seismic parameters estimated from the seismograms of 1.6-s time window from 0.2 s before the first *P*-pulse arrival for used 51 events.

Origin Time	*M*	*R*, km	*Mo*, Nm	*E*, J	*R*
1989/7/4 14:16	2.9	35.625	7.76E+12	7.77E+06	0.7589
1989/7/4 14:23	2.6	35.828	4.73E+12	3.50E+06	0.7457
1989/7/4 14:24	3.0	35.101	1.89E+13	4.13E+07	0.9947
1989/7/4 14:46	2.4	35.092	2.76E+12	2.23E+06	1.1077
1989/7/4 15:52	2.5	35.618	6.50E+12	1.01E+07	1.3092
1989/7/4 17:04	2.5	35.670	5.65E+12	1.02E+07	1.6453
1989/7/4 17:42	2.6	36.106	1.14E+13	1.60E+07	0.8529
1989/7/4 18:43	3.3	34.774	1.57E+13	4.62E+07	1.4915
1989/7/4 19:06	2.5	35.752	1.06E+13	3.83E+07	2.2932
1989/7/4 19:30	2.7	35.969	1.73E+13	1.17E+08	3.2185
1989/7/4 19:31	2.9	35.492	1.95E+13	4.91E+07	1.1259
1989/7/4 21:41	3.5	36.343	2.32E+13	6.83E+07	1.1873
1989/7/4 23:40	2.7	35.761	6.43E+12	7.24E+06	0.9509
1989/7/5 0:08	3.0	34.723	1.87E+13	9.98E+07	2.4433
1989/7/5 0:34	3.1	36.003	1.98E+13	1.70E+08	3.8164
1989/7/5 1:39	3.1	36.373	1.51E+13	4.21E+07	1.4427
1989/7/5 2:41	2.9	35.466	3.06E+13	1.13E+08	1.2733
1989/7/5 5:36	3.3	35.363	2.31E+13	3.09E+07	0.5444
1989/7/5 18:04	2.5	36.068	2.43E+12	4.28E+06	2.6023
1989/7/5 22:58	2.9	34.958	7.58E+12	6.97E+06	0.7060
1989/7/5 23:05	2.4	34.881	2.73E+12	3.70E+06	1.8751
1989/7/6 3:26	3.1	36.426	2.02E+13	5.06E+07	1.0945
1989/7/6 3:46	2.7	35.297	6.08E+12	4.20E+06	0.6023
1989/7/6 5:45	3.3	35.551	1.78E+13	2.70E+07	0.7157
1989/7/6 5:59	3.1	35.643	9.39E+12	8.30E+06	0.6001
1989/7/6 6:29	3.0	35.821	2.39E+13	2.33E+07	0.3874
1989/7/6 6:38	3.4	35.830	2.30E+13	3.45E+07	0.6102
1989/7/6 6:46	2.7	36.437	8.59E+12	1.48E+07	1.2330
1989/7/6 7:15	3.0	35.957	2.88E+13	1.66E+08	2.0515
1989/7/6 7:37	2.6	35.942	6.73E+12	5.03E+06	0.6134
1989/7/6 12:16	2.5	36.439	1.27E+13	4.58E+07	2.0517
1989/7/6 13:14	2.7	35.628	1.17E+13	7.46E+06	0.3818
1989/7/6 13:28	2.9	34.915	2.00E+13	4.00E+07	0.8796
1989/7/6 13:30	2.6	36.294	7.12E+12	5.58E+06	0.6230
1989/7/7 1:38	3.3	34.581	3.52E+13	2.08E+08	1.8824
1989/7/7 4:16	3.0	34.352	3.20E+13	7.46E+07	0.7855
1989/7/8 5:07	2.6	34.918	8.94E+12	8.76E+06	0.6844
1989/7/8 7:12	3.1	35.568	9.85E+12	1.87E+07	1.2570
1989/7/8 7:12	3.4	35.599	2.10E+13	3.34E+07	0.6820
1989/7/8 20:49	2.5	35.330	7.40E+12	4.18E+06	0.4390
1989/7/8 21:14	3.1	34.685	3.71E+13	7.39E+07	0.6161
1989/7/9 3:49	2.8	34.774	1.50E+13	2.32E+07	0.8003
1989/7/9 8:35	2.9	34.334	1.53E+13	3.10E+07	1.0393
1989/7/9 8:51	3.1	34.106	3.07E+13	5.96E+07	0.6678
1989/7/9 12:17	2.6	34.632	6.00E+12	3.17E+06	0.4641
1989/7/9 12:42	2.5	34.340	3.31E+12	1.42E+06	0.5301
1989/7/9 21:04	3.2	33.747	2.05E+13	3.85E+07	0.8174
1989/7/9 21:58	2.7	34.644	8.31E+12	9.80E+06	0.8584
1989/7/9 23:24	2.7	34.393	6.46E+12	6.70E+06	0.8728
1989/7/12 5:52	2.6	34.461	5.20E+12	9.47E+06	1.7375
1989/7/14 13:40	2.5	35.316	6.59E+12	1.05E+07	1.3277

might seem preferable to monitor the stress state. However, an accurate estimate of $\Delta\sigma$ from the corner frequency requires the corner frequency determined with the Fourier analysis over a wide band of frequency. For relatively small earthquakes, such as those in the present study, phase duration is too short for us to have an enough number of samples, not allowing us to accurately locate the corner frequency on the Fourier spectrum.

The ratio of radiated seismic energy E to seismic moment Mo is another measure of the stress drop in an earthquake. Wyss and Brune (1968) define the apparent stress, σ_a, as

$$\sigma_a = \frac{E\mu}{Mo}, \tag{7}$$

where μ is the shear modulus. Savage and Wood (1971) described σ_a as

$$\sigma_a = \frac{\Delta\sigma}{2} + \sigma_r - \sigma_f, \tag{8}$$

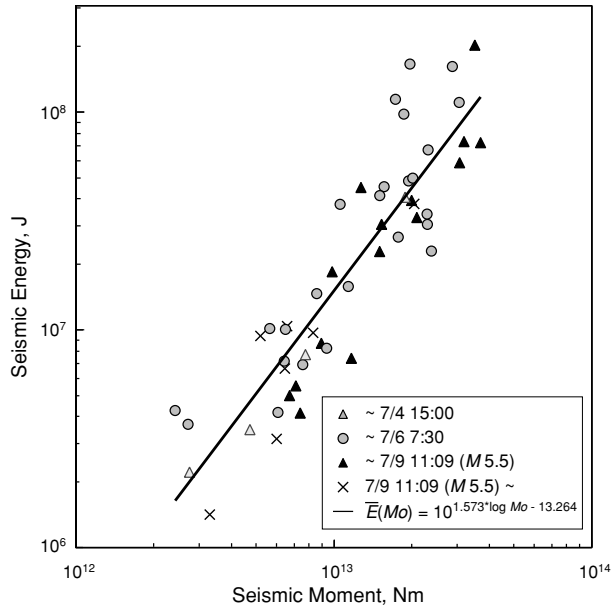

Fig. 6. The relationship between E and Mo obtained using the seismograms of a 1.6-s time window from 0.2 s before the first P-pulse arrival. A line shows the estimated $\overline{E}(Mo)$. Gray triangles, gray circles, black triangles, and crosses represent earthquakes that occurred in period 1 (~ July 4, 15:00), period 2 (~ July 6, 7:30), period 3 (~ July 9, 11:09; M 5.5), and period 4 (after M 5.5), respectively.

where $\Delta\sigma$, σ_r, and σ_f represent mean stress drop, final stress level, and mean frictional stress, respectively. If we plot E versus Mo for all events in the area of interest, we obtain the following empirical standard relationship by regression analysis:

$$\overline{E}(Mo) = 10^{a\log Mo+b}, \tag{9}$$

where $\overline{E}(Mo)$ is the energy expected for a given seismic moment, and the constants a and b are empirically determined for the area of interest. Some of recent studies (e.g., Iio, 1986; Kanamori *et al*., 1993; Abercrombie, 1995) have shown that a in Eq. (9) is significantly larger than unity (in our case, $a \approx 1.57$ as shown in Fig. 6), hence there is an increase in σ_a with Mo. Therefore earthquakes of different magnitudes cannot be used to investigate temporal variations in σ_a. However, Ide and Beroza (2001) pointed out the a value larger than unity in the previous studies was caused by underestimation of E especially for the small earthquakes because of the limited band of frequency range. They added missing energy by extrapolation of high-frequency asymptote, and showed σ_a is in the range of 0.1 and 10 MPa over the entire range of earthquake size. Yamada *et al*. (2005) directly estimated seismic moment and seismic energy of the seismic events ($0.8 < M < 1.4$) occurred in a deep South African gold mine from the seismograms recorded with sufficiently high sampling frequency (15 kHz), and showed sa is also in the range of 1 and 10 MPa.

So, it is possible that the sampling frequency of 80 Hz at NSI is not high enough for the events ($2.4 < M < 3.5$), causing the underestimation in energy. To address the problem, then, we introduce a substitutive stress parameter, energy index (*EI*) by van Aswegen and Butler (1993), which allows a in Eq. (9) is not around unity:

$$EI = \frac{E}{\overline{E}(Mo)}, \tag{10}$$

We then calculate the energy index *EI* using Eqs. (9) and (10) (Table 1). The relationship between Mo and E and estimated $\overline{E}(Mo)$ are shown in Fig. 6.

Here we demonstrate the narrow-band *EI* in this study corresponds well to the apparent stress properly estimated with a full-band seismogram. We set variable levels of Mo from $10^{12.4}$ Nm to $10^{13.6}$ Nm, and calculate AoR/F^P from Eq. (4). Also, assuming that $\Delta\sigma = 2$ MPa and according to Eq. (6), we calculate a reference corner frequencies fc for each Mo. We add the random perturbation of $\pm 20\%$ to the reference frequency obtaining a variable set of Mo and f_c. Neglecting the anelastic attenuation in Eq. (3), we have:

$$\dot{U}(f) = \frac{Ao \cdot f}{(1 + f/f_c)^2}, \tag{11}$$

Then, estimated seismic energy is represented as

$$\begin{aligned} E(F_{\max}) &= \int_{F_{\min}}^{F_{\max}} \frac{4\pi R^2 \rho\alpha}{F^{P\,2}} [\dot{U}(f)]^2 df \\ &= 4\pi\rho\alpha \left(\frac{AoR}{F^P}\right)^2 \int_{F_{\min}}^{F_{\max}} \left[\frac{f}{(1 + f/f_c)^2}\right]^2 df, \end{aligned} \tag{12}$$

Specifying $F_{\min} = 0.01$ Hz, we compare the frequency-domain integration of the squared far-field velocity over the wide and narrow frequency-bands; $F_{\max} = 1000$ Hz (wide range) and $F_{\max} = 20$ Hz (narrow range, this study), respectively.

We hereinafter refer to the E thus obtained as E (1000 Hz) and E (20 Hz), and the *EI* as *EI* (1000 Hz) and *EI* (20 Hz), respectively. As shown in Fig. 7, a in Eq. (9) is around unity for E (1000 Hz), suggesting *EI* (1000 Hz) is effectively close to the full-band apparent stress. In contrast, a for E (20 Hz) is significantly larger (1.41), much as in our study (1.57). However, note that a higher *EI* (20 Hz) corresponds well to a higher *EI* (1000 Hz), as shown in Fig. 8. Consequently, the *EI* (20 Hz) in our analysis corresponds well to the full-band apparent stress over the magnitude range of our analysis although some scatter is seen.

If we assume that σ_r and σ_f in Eq. (8) are equal (Orowan, 1960), then we obtain

$$E = \frac{\Delta\sigma}{2\mu} Mo, \tag{13}$$

which is the same approximate relationship given under the dry-friction law by Kostrov (1974). The value of μ can be assumed to be constant in a given region of interest. If we also assume that final stress level is almost uniform in the source region of the largest earthquake, then the temporal variation of the initial stress level can be estimated from the temporal variation of $\Delta\sigma$. Hence, calculating the *EI* of foreshocks whose magnitude range is narrow, which can be a reliable substitution of real σ_a and $\Delta\sigma$, allows us to monitor the temporal change in stress level in the source region, even if the effective frequency range is limited.

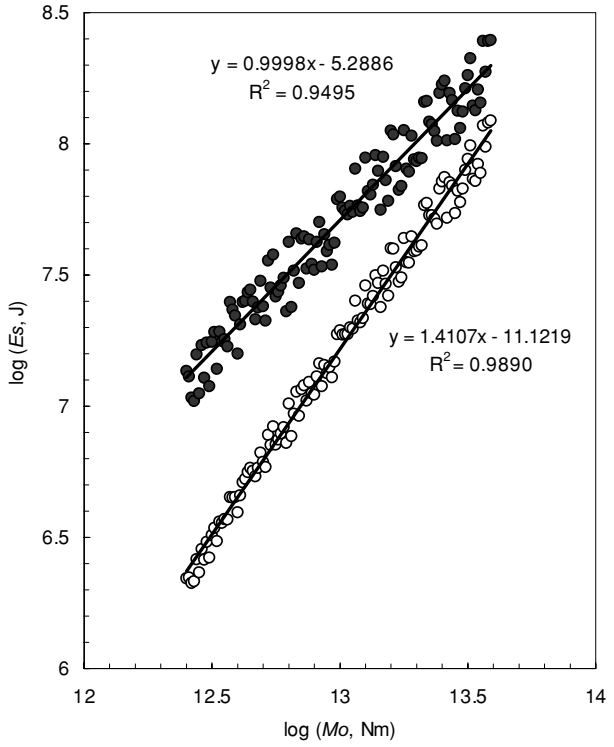

Fig. 7. The relationship between E and Mo of synthetic data. Lines show the estimated $\overline{E}(Mo)$. Solid and open circles represent the case that $F_{\max} = 1000$ Hz and 20 Hz, respectively.

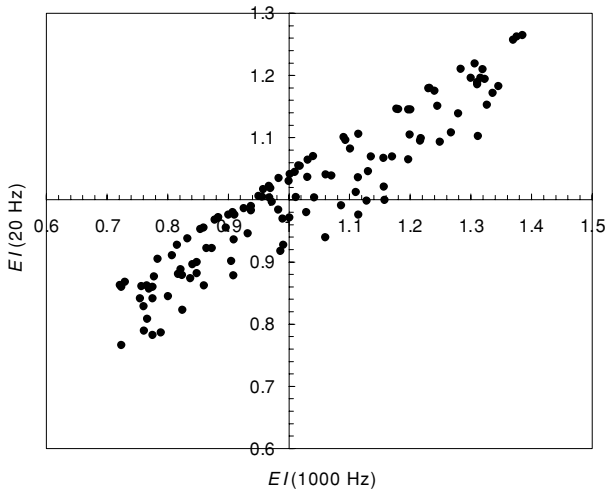

Fig. 8. The relationship between *EI* (20 Hz) and *EI* (1000 Hz) that is equivalent to the apparent stress.

6. Temporal Variation in *EI*

We calculate the energy index *EI* for 51 earthquakes that occurred between July 4 and July 14, 1989 in the swarm region east of the Izu Peninsula (Table 1). Figure 9 shows the temporal variation in *EI* (a raw value, a 10-event running mean and median in Figs. 9(a), (b), and (c), respectively) and the cumulative frequency of earthquake (Fig. 9(d)). A 10-event window is the narrowest window that covers the entire target volume.

Seismic activity in the study region began suddenly on July 4 (Fig. 9(d)), and *EI* increased and remained high for

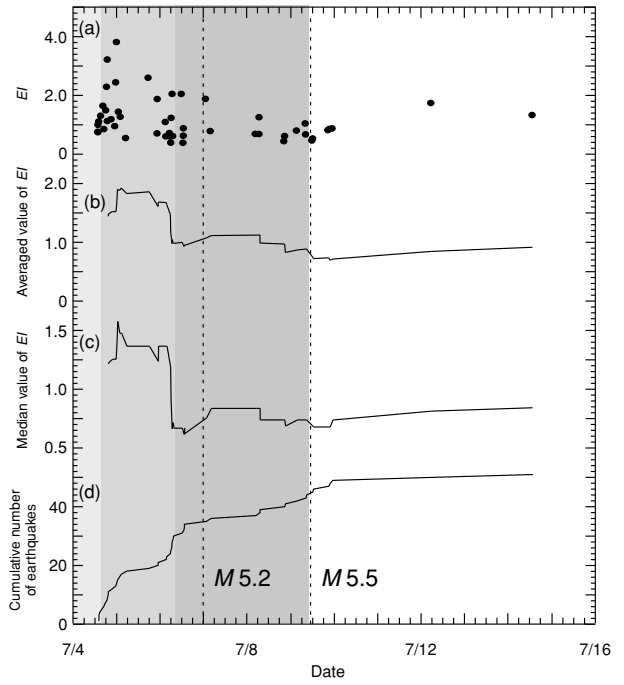

Fig. 9. Temporal variation in parameters. (a) Raw value of *EI*. (b) Running mean of *EI* (10 events). (c) Running median value of *EI* (10 events). (d) Cumulative number of earthquakes.

about one and a half days. *EI* then decreased early on July 6 (Figs. 9(b) and (c)), before the *M* 5.2 earthquake occurred early on July 7. Thereafter, *EI* remained relatively low even after the *M* 5.5 earthquake on July 9 (Figs. 9(b) and (c)). Regardless of the width of the moving window, *EI* in the target region increased when the seismicity increased on July 4, started to decrease from July 6, and remained low until the termination of the swarm.

Figure 6 shows that the E values are higher from 15:00 (LT) on July 4 to 7:30 (LT) on July 6, whereas lower from 7:30 (LT) on July 6 to the *M* 5.5 earthquake than $\overline{E}(Mo)$, the expected values for given Mo. We then performed the t-test for the null hypothesis that the *EI* was lower from 15:00 (LT) on July 4 to 7:30 (LT) on July 6 than from 7:30 (LT) on July 6 to the *M* 5.5 earthquake. We are able to reject this null hypothesis with a significance level of 0.015%, and so the decrease in *EI* on early July 6 can be considered statistically significant.

7. Discussion

We observe an increase in *EI* early on July 4, 1989 in the source region of the *M* 5.5 earthquake, and decrease in *EI* there early on July 6, before the *M* 5.2 earthquake occurred early on July 7, and the *M* 5.5 earthquake occurred on July 9.

7.1 Rupture directivity effect

If the rupture propagates toward a station, the seismic energy E estimated from the seismogram recorded at the station will be overestimated (rupture directivity effect), but the seismic moment Mo is not affected. In such cases, *EI* will be overvalued. If high *EI* values result from the overestimation of E due to rupture directivity effect, the pulse width of *P*- or *S*-wave for high *EI* events is much shorter

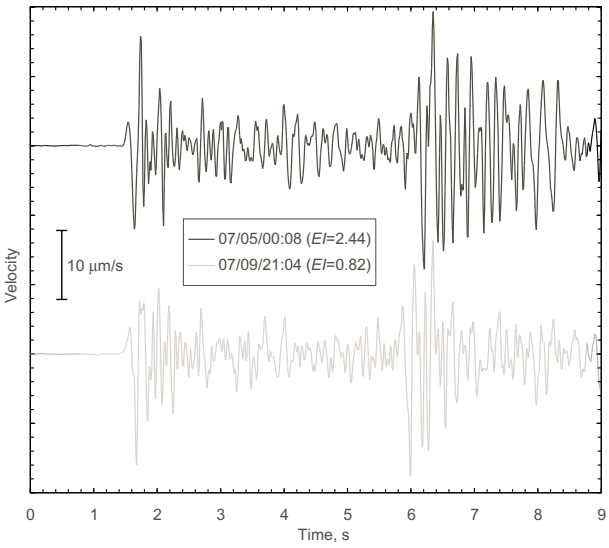

Fig. 10. Vertical component of velocity seismograms for typical earthquakes with similar *Mo*, but significantly different *EI*. Black and gray seismograms represent a high *EI* (2.44) event occurred at 0:08 on July 5, and a low *EI* (0.82) event occurred at 21:04 on July 9, respectively.

than that for low *EI* events, and also the pulse width of *S*-wave is significantly shorter than that of *P*-wave for high *EI* events. Figure 10 is one of the typical velocity seismogram examples for the events with similar *Mo* but significantly different *EI*. As shown in Fig. 10, all of the pulse widths of *P*- and *S*-waves are nearly identical independently of the significant difference in *EI*. This is true for other pairs of events with similar *Mo* and different *EI*. Then, we conclude that the high *EI* values are not caused by rupture directivity effects.

7.2 Comparison with geodetic data

The tiltmeters at station ITO (Fig. 1) recorded a rapid acceleration on the morning of July 4, coincident with the onset of seismic activity in the whole swarm region (both eastern and western groups) (Yamamoto *et al*., 1991). In addition, the dilatometer at station HIZ (Fig. 1) detected a large contraction (Earthquake Prediction Information Division, 1990). Both changes are shown in Fig. 11. These deformations can be modeled well as the elastic response to the continuous opening of a vertical crack (the white line in Fig. 1) to a thickness of about 1 m (Okada and Yamamoto, 1991). Our observation that *EI* also increased on July 4, suggests that stress increased in the western region of swarm activity (the source region of *M* 5.5), due to external loading by the crack opening. However, *EI* started to decrease on July 6, despite the increasing tilt and dilatation, which suggests that the decrease in *EI* was independent of the external loading. Stations ITO and HIZ were located about 7 km and 15 km, respectively, from the epicenter of the *M* 5.5 earthquake. Therefore, the decrease in *EI* starting on July 6 implies the decrease in stress only in the source region of the *M* 5.2 and 5.5 earthquakes, which suggests the onset of yielding. Meanwhile the external loading was continued in the entire swarm region, associated with the monotonic opening of the crack that eventually resulted in a submarine volcanic eruption on July 13.

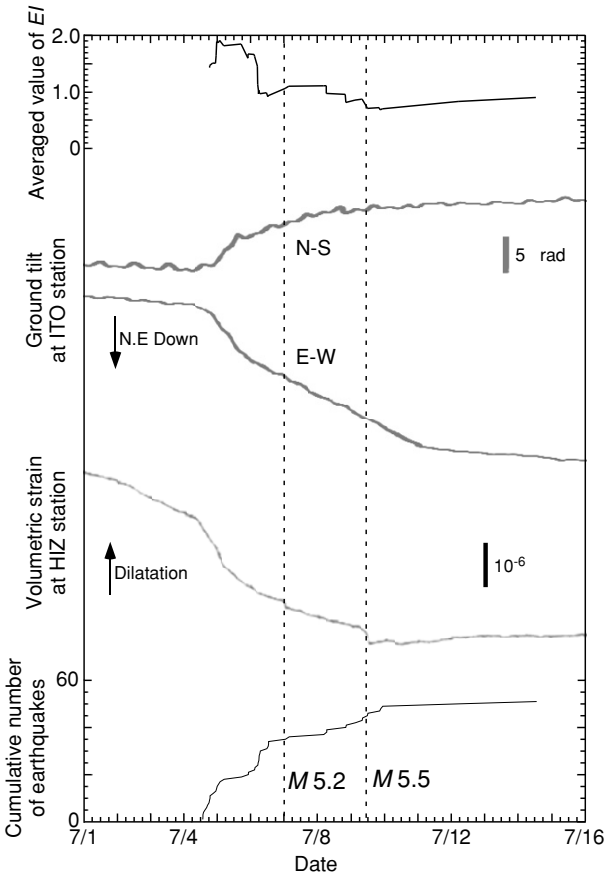

Fig. 11. Temporal variation in ground tilt at station ITO (after Yamamoto *et al*., 1991) and volumetric strain at station HIZ (after Earthquake Prediction Information Division, 1990). Also shown are the running mean of *EI* and the cumulative number of earthquakes.

7.3 Comparison with South African gold mines

In South African gold mines, a decrease in *EI* has sometimes been observed to precede major seismic events induced by mining activities (e.g., Mendecki, 1997; van Aswegen *et al*., 1997; Sato, 2000; Ogasawara *et al*., 2002). Sato (2000) and Ogasawara *et al*. (2002) showed a precursory *EI* decrease about a half-day before an $M\sim2$ earthquake. It is possible that the longer precursory decrease of a few days that we observe indicates a relationship between the duration of the low *EI* and the size of the subsequent main shock. Sato (2000) and Ogasawara *et al*. (2002) also detected an *EI* increase simultaneous with strain acceleration, indicating a concentration of stress by mining. Ishii *et al*. (1998) detected strain acceleration about five days before the $M\sim2$ earthquake from 5×10^{-7} /day to 7×10^{-6} /day. For Izu in 1989, the strain rate increased on July 1 from 9×10^{-9} /day to 2×10^{-7} /day, and on July 4 to 1.3×10^{-6} /day. The data from Izu and South Africa suggest that a strain acceleration greater than ten times was enough to significantly increase seismicity, and to induce yielding and a consequent major earthquake, even though the mechanisms of strain acceleration were different between magma intrusion at Izu and mining in South Africa.

7.4 Rapid stress accumulation and yielding prior to the largest earthquakes

Large earthquakes related to volcanic activity are frequently preceded by active foreshock sequences. Such was the case for the 1989 earthquake swarm off the eastern Izu Peninsula. This is unusual for natural earthquakes of tectonic origin (e.g., Abercrombie and Mori, 1996; Maeda, 1999). Since the 1974 Izu-Hanto-Oki earthquake (M = 6.9), the recurrence time of earthquakes with $M \geq 5.5$ related to volcanic activity has been about 10 years in and around Izu Peninsula, while the recurrence of crustal earthquakes of tectonic origin in Japan is about a thousand years or longer (e.g., Sugiyama, 2000). The stress accumulation rate in the Izu region is thus about ten times as high as in the source regions of crustal earthquakes of tectonic origin in Japan, if the Izu rate had remained constant. Similar foreshock activity was observed in the laboratory, where the stress accumulation rate is much higher than it was at Izu (e.g., Meredith *et al*., 1990; Kawakata and Shimada, 1995). Thus high foreshock activity may be related to a high rate of stress accumulation, as suggested by Dieterich (1994), Dieterich *et al*. (2000), and Toda *et al*. (2002).

At a certain stress level, local yielding starts to occur in parts of the rock mass with low strength. As stress accumulates further, regions with higher strength will also yield. At this stage, earthquake stress drops would be expected to increase, consistent with our observed increase in the *EI*. When the bulk strength is reached in a source region capable of producing a major earthquake, bulk yielding begins. At this stage, accumulated stress is gradually released, and the stress drop and *EI* of earthquakes in the region would be expected to decrease.

Alternatively, if the strength in the source region is uniform, an increase in the *EI* can be explained by acceleration in stress accumulation, and a decrease in the *EI* would result from bulk yielding. In the case of the 1989 swarm, a magma intrusion caused a major change in the rate of stress accumulation from July 4 (Fig. 11). This stress accumulation rate was over ten times greater than the rate in the days preceding this eight-day interval. Lankford (1981) and Kato *et al*. (1992) showed that yielding stress increases as stress accumulation accelerates in the laboratory.

These are possible mechanisms for *EI* increase and decrease prior to M 5.2 and 5.5 events. We therefore propose a mechanism of precursory change in *EI* for the major earthquakes in the 1989 earthquake swarm off the eastern Izu Peninsula as follows:

1) On July 4, 1989, strain accumulation accelerated in the eastern portion of the source region of the major earthquakes (M 5.2 and 5.5), due to magma intrusion, and local yielding started in the region with the lowest yielding strength followed by yielding in the stronger region. The *EI* and stress drop of earthquakes that occurred in this stage increased.

2) Further strain accumulation due to magma intrusion caused the whole source region of the M 5.5 earthquake to yield on July 6, and stress quasi-statically decreased because of anelastic deformation. Earthquakes occurring at this stage (the earthquake development stage) had smaller stress drops than those in the previous stage, so that *EI* decreased.

3) After occurrence of the M 5.2 earthquake on early July 7, the M 5.5 earthquake took place in the vicinity of the strong asperity on July 9, and the accumulated stress around the M 5.5 source region was released. After the M 5.5 earthquake, the *EI* remained at a constant level.

8. Conclusions

We examine stress change prior to the largest earthquakes (M = 5.2 and 5.5) in the 1989 earthquake swarm off the eastern Izu Peninsula in Japan using energy index *EI*, which are estimated from seismic moment and seismic energy. *EI* is an estimate of stress state that is independent of *Mo* unlike the apparent stress estimated from seismograms with a limited band of frequency range. We observe a stress increase in the source region of the M 5.5 earthquake, coincident with sudden changes in tilt and dilatation outside of the swarm region, that indicated the strain accumulation due to external loading caused by opening of the vertical crack. We then observe an *EI* decrease a few days prior to the major events, suggesting that yielding took place only in the source region and that stress was reduced during the earthquake development process. We should note that denser observations over a wider dynamic range will enable us to more clearly observe the earthquake development process (i.e., yielding and stress decrease) from the seismogram analyses, in cases where the foreshock activity or background seismicity is strong enough.

Acknowledgments. We thank the staff of the National Research Institute for Earth Science and Disaster Prevention for providing seismograms and mechanism solutions. We are also grateful to Dr. Shiro Ohmi, Dr. Yoshihisa Iio, and Dr. Tomotaka Iwata for their helpful suggestions regarding waveform analysis. We are especially indebted to Dr. Satoshi Ide and Dr. Rachel E. Abercrombie whose constructive suggestions and comments substantially improved our manuscript. We wish to express our gratitude to Dr. Yoshimitsu Okada and an anonymous referee for their critical comments that are useful for the improvement of our manuscript. The GMT software of Wessel and Smith (1995) was used to create Fig. 1.

References

Abercrombie, R. E., Earthquake Source Scaling Relationships from −1 to 5 M_L using seismograms recorded at 2.5-km depth, *J. Geophys. Res.*, **100**, 24015–24036, 1995.

Abercrombie, R. E. and J. Mori, Occurrence patterns of foreshocks to large earthquakes in the western United States, *Nature*, **381**, 303–307, 1996.

Aki, K. and P. G. Richards, *Quantitative Seismology*, Freeman, San Francisco, 1980.

Azimi, Sh. A., A. V. Kalinin, V. V. Kalinin, and B. L. Pivovarov, Impulse and transient characteristics of media with linear and quadratic absorption laws, *Izv. Earth Phys.* (Engl. Tlansl. by F. Goodspeed), **2**, 88–93, 1968.

Boatwright, J., A spectral theory for circular seismic sources; simple estimates of source dimension, dynamic stress drop, and radiated seismic energy, *Bull. Seismol. Soc. Am.*, **70**, 1–26, 1980.

Brudy, M., M. D. Zoback, K. Fuchs, F. Rummel, and J. Baumgartner, Estimation of the complete stress tensor to 8 km depth in the KTB scientific drill holes: Implications for crustal strength, *J. Geophys. Res.*, **102**, 18453–18475, 1997.

Brune, J. N., Tectonic stress and the spectra of seismic shear waves from

earthquakes, *J. Geophys. Res.*, **75**, 4997–5002, 1970.
Burridge, R. and L. Knopoff, Model and theoretical seismicity, *Bull. Seismol. Soc. Am.*, **57**, 341–371, 1967.
Carlson, J. M. and J. S. Langer, Properties of earthquakes generated by fault dynamics, *Phys. Rev. Lett.*, **62**, 2632–2635, 1989.
COMRO; Chamber of Mines Research Organization, in *An Industry Guide to Methods of Ameliorating the Hazards of Rockfalls and Rockbursts, Chamber of Mines of South Africa*, 114 pp, 1988.
Dieterich, J. H., A constitutive law for rate of earthquake production and its application to earthquake clustering, *J. Geophys. Res.*, **99**, 2601–2618, 1994.
Dieterich, J., V. Cayol, and P. Okubo, The use of earthquake rate change as a stress meter at Kilauea volcano, *Nature*, **408**, 457–460, 2000.
Earthquake Prediction Information Division, Japan Meteorological Agency, Seismic Activity off East Coast of Izu-Peninsula, 1989 and Strain Changes Observed by the Borehole Strainmeter, *Rep. Coord. Comm. Earthq. Predict.*, **43**, 284–289, 1990 (in Japanese).
Eshelby, J. D., The determination of the elastic field of an ellipsoidal inclusion and related problems, *Proc. R. Soc. London A*, **241**, 376–396, 1957.
Fukuyama, E., S. Kinoshita, and F. Yamamizu, Unusual high-stress drop subevent during the M5.5 earthquake, the largest event of the 1989 Itooki swarm activity, *Geophys. Res. Lett.*, **18**, 641–644, 1991.
Gibowicz, S. J. and A. Kijko, *An Introduction to Mining Seismology*, Academic Press, San Diego, 1994.
Ide, S. and G. C. Beroza, Does apparent stress vary with earthquake size?, *Geophys. Res. Lett.*, **28**, 3349–3352, 2001.
Iio, Y., Scaling relation between earthquake size and duration of faulting for shallow earthquakes in seismic moment between 10^{10} and 10^{25} dyne·cm, *J. Phys. Earth*, **34**, 127–169, 1986.
Ishii, H., T. Ohkura, and The Research Group for Semi-controlled Experiment for Earthquake Generation Process in South African Deep Gold Mine, Strain monitoring and earthquake generation in South African deep gold mine, *Chikyu Monthly*, **20**, 419–422, 1998 (in Japanese).
Kanamori, H., J. Mori, E. Hauksson, T. H. Heaton, L. K. Hutton, and L. M. Jones, Determination of earthquake energy release and ML using TERRAscope, *Bull. Seismol. Soc. Am.*, **83**, 330–346, 1993.
Kato, N., K. Yamamoto, H. Yamamoto, and T. Hirasawa, Strain-rate effect on frictional strength and the slip nucleation process, *Tectonophys.*, **211**, 269–282, 1992.
Kawakata, H. and M. Shimada, Frequency-magnitude relation of AE in fracture process of rocks at high confining pressures, *Proc. 8th Int. Congr. Rock Mech.*, **1**, 207–210, 1995.
Kawakata, H., A. Cho, T. Kiyama, T. Yanagidani, K. Kusunose, and M. Shimada, Three-dimensional observations of faulting process in westerly granite under uniaxial and triaxial conditions by X-ray CT scan, *Tectonophys.*, **313**, 293–305, 1999.
Keilis-Borok, V. I., Investigation of the mechanism of earthquakes, *Sov. Res. Geophys.* (English Tlansl.), **4**, 29, 1960.
Kostrov, V. V., Seismic moment and energy of earthquakes, and seismic flow of rock, *Izv. Earth Phys.* (Engl. Tlansl. by F. Goodspeed), **1**, 13–21, 1974.
Lankford, J., The role of tensile microfracture in the strain rate dependence of compressive strength of fine-grained limestone-analogy with strong ceramics, *Int. J. Rock Mech. Min. Sci. & Geomech. Abstr.*, **18**, 173–175, 1981.
Madariaga, R., Dynamics of an expanding circular fault, *Bull. Seismol. Soc. Am.*, **66**, 639–666, 1976.
Maeda, K., Time distribution of immediate foreshocks obtained by a stacking method, *Pure Appl. Geophys.*, **155**, 381–394, 1999.
Matsumura, S., T. Ohkubo, and M. Imoto, Seismic swarm activity in and around the Izu Peninsula preceding the volcanic eruption of July 13, 1989, *J. Phys. Earth*, **39**, 93–106, 1991.
Mendecki, A. J., Quantitative seismology and rock mass stability, in *Seismic Monitoring in Mines*, edited by A. J. Mendecki, pp. 178–219, Chapman and Hall, London, 1997.
Meredith, P. G., I. G. Main, and C. Jones, Temporal variation in seismicity during quasi-static and dynamic rock failure, *Tectonophys.*, **175**, 249–268, 1990.
Ogasawara, H., S. Sato, S. Nishii, K. Mino, and Research Group for Earthquake Generation Experiment in South African Deep Gold Mines, Temporal variation of seismic parameters associated with an $Mw\sim2$ event monitored at 100∼200 m distance, in *Seismogenic Process Monitoring*, edited by H. Ogasawara, T. Yanagidani, and M. Ando, pp. 173–184, Balkema, Rotterdam, 2002.
Ogasawara, H., J. Takeuchi, N. Shimoda, H. Ishii, S. Nakao, G. van Aswegen, A. J. Mendecki, A. Cichowicz, R. Ebrahim-Trollope, H. Kawakata, Y. Iio, T. Ohkura, M. Ando, and the Research Group for Semi-controlled Earthquake-generation Experiments in South African deep gold mines, High-resolution Strain Monitoring During $M\sim2$ Events in a South African Deep Gold Mine in Close Proximity to Hypocentres, *Proc. 6th Int. Symp. on Rockburst and Seismicity in Mines*, 385–391, 2005.
Ohnaka, M., Y. Kuwahara, K. Yamamoto, and T. Hirasawa, Dynamic breakdown process and the generating mechanism for high-frequency elastic radiation during stick-slip instability, in *Earthquake Source Mechanics, Maurice Ewing Ser. 6*, edited by S. Das, J. Boatwright, and C. H. Scholz, pp. 13–24, American Geophysical Union, Washington, D.C. 1986.
Okada, Y. and E. Yamamoto, Dyke intrusion model for the 1989 seismovolcanic activity off Ito, central Japan, *J. Geophys. Res.*, **96**, 10361–10376, 1991.
Orowan, E., Mechanism of seismic faulting in rock deformation, *Geol. Soc. Am. Mem.*, **79**, 323–345, 1960.
Rudnicki, J. W., Physical models of earthquake instability and precursory processes, *Pure Appl. Geophys.*, **126**, 531–554, 1988.
Sato, S., Inference of Earthquake Generation Process from Energy Index and Apparent Volume, Master Thesis, Ritsumeikan Univ., Shiga, Japan, 2000 (in Japanese).
Savage, J. C. and M. D. Wood, The relationship between apparent stress and stress drop, *Bull. Seismol. Soc. Am.*, **61**, 1381–1388, 1971.
Simmons, G., R. W. Siegfried, and M. Feves, Differential strain analysis: A new method for examining cracks in rocks, *J. Geophys. Res.*, **79**, 4383–4385, 1974.
Sugiyama, Y., Research on earthquake potential evaluation by active faults, *Bull. Geol. Surv. Japan*, **51**, 379–389, 2000 (in Japanese with English Abstract).
Suzuki, H., R. Ikeda, T. Mikoshiba, S. Kinoshita, H. Sato, and H. Takahashi, Deep well logs in the Kanto-Tokai area, review, *Res. Disas. Prev.*, **65**, 1–162, 1981 (in Japanese with English Abstract).
Teufel, L. W., Determination of In-situ Stress from Anelastic Strain Recovery Measurements of Oriented Core, *Proc. 1983 SPE/DOE Joint Symp. on Low Permeability Gas Reservoirs*, 421–430, 1983.
Toda, S., R. S. Stein, and T. Sagiya, Evidence from the AD 2000 Izu island earthquake swarm that stressing rate governs seismicity, *Nature*, **419**, 58–61, 2002.
van Aswegen, G. and A. Butler, Applications of quantitative seismology in South African gold mines, in *Rockbursts and Seismicity in Mines 93*, edited by R. P. Young, pp. 261–266, Balkema, Rotterdam, 1993.
van Aswegen, G., A. J. Mendecki, and C. Funk, Application of quantitative seismology in mines, in *Seismic Monitoring in Mines*, edited by A. J. Mendecki, pp. 220–245, Chapman and Hall, London, 1997.
Wessel, P. and W. H. F. Smith, New version of the generic mapping tools released, *Eos Trans. AGU*, **76**, 329, 1995.
Wyss, M. and J. N. Brune, Seismic moment, stress, and source dimensions for earthquakes in the California-Nevada region, *J. Geophys. Res.*, **73**, 4681–4694, 1968.
Yamada, T., J. J. Mori, S. Ide, H. Kawakata, Y. Iio, and H. Ogasawara, Radiation efficiency and apparent stress of small eartqhaquake in a South African gold mine, *J. Geophys. Res.*, **101**(B1), 1305, doi:10.1029/2004JB003221, 2005.
Yamamoto, E., Y. Okada, and T. Ohkubo, Ground tilt changes preceding the 1989 submarine eruption off Ito, Izu Peninsula, *J. Phys. Earth*, **39**, 165–176, 1991.
Zang, A., H. Berckhemer, and M. Lienert, Crack closure pressures inferred from ultrasonic drill-core measurements to 8 km depth in the KTB wells, *Geophys. J. Int.*, **124**, 657–674, 1996.

H. Kawakata (e-mail: kwkt@drs.dpri.kyoto-u.ac.jp), H. Ogasawara, S. Sekiguchi, S. Uyama, and K. Mino